Computational analysis of resisting marine FRP divisions exposed to fire. Application to the analysis of ship structures.

Rafael Pacheco-Blazquez*[,1,2], Daniel Di Capua[1,2], Julio García-Espinosa[1,3], Ovidi Casals[4], Tuula Hakkarainen[5], Alexandra Tissari[5] and Antti Korkealaakso[5]

[1]Centre Internacional de Mètodes Numèrics a l'Enginyeria (CIMNE)
Edifici C1, Campus Norte, UPC, Gran Capitán s/n, 08034 Barcelona, Spain
e-mail: dicapua@cimne.upc.edu, julio@cimne.upc.edu
*corresponding author: rpacheco@cimne.upc.edu

[2]Departament de Resistència de Materials i Estructures a l'Enginyeria (RMEE)
Universitat Politècnica de Catalunya (UPC)
Campus Diagonal Besòs, 08019 Barcelona, Spain

[3]Escuela Técnica Superior de Ingenieros Navales (ETSIN)
Universidad Politécnica de Madrid (UPM)
Av. de la Memoria, 4, 28040 Madrid, Spain

[4]Compass Ingeniería y Sistemas S.A.
C/ Gran Capità s/n, Edifici B0, Campus Nord UPC, 08034 Barcelona, Spain
e-mail: ovidi.casals@compassis.com

[5]VTT Technical Research Centre of Finland Ltd, Finland (VTT)
Kemistintie 3, P.O. Box 1000, FI-02044 VTT, Espoo, Finland
e-mail: Tuula.Hakkarainen@vtt.fi, Alexandra.Tissari@vtt.fi, Antti.Korkealaakso@vtt.fi

ABSTRACT

This paper describes the research performed within the scope of H2020 project NICESHIP in the development of suitable thermo-mechanical framework to analyse composite structures under fire loads. The framework couples the thermo-mechanical model that is detailed in the paper with the Fire Dynamics Simulator (FDS) in order to obtain the adiabatic temperature needed as input for thermal model. The thermo-mechanical model uses the adiabatic temperature to estimate the temperature profile across the thickness of each quadrilateral shell element and also takes into account the pyrolysis effect. The composite constitutive model employed is the so-called Serial/Parallel Rule of Mixtures (SPROM) and has been modified to take into account the thermal expansion. Finally the thermo-mechanical model is validated against two literature tests and then the developed framework of fire collapse analysis is illustrated by a marine real application of a fire case scenario in the superstructure of a containership where steel and FRP divisions are analysed.

Keywords: Fire Safety, Fire Collapse, Fire Dynamics , Thermo-mechanical, Composites, Marine Structures

NOMENCLATURE

ρ	density $\left(\frac{\text{kg}}{\text{m}^3}\right)$
$\mathbf{n}$	normal
l_t	thickness (m)
v	velocity $\left(\frac{\text{m}}{\text{s}}\right)$
ϕ	volume fraction
Ω	domain
E_a	activation energy for decomposition reaction of polymer matrix $\left(\frac{\text{J}}{\text{kmol}}\right)$
k	through-thickness thermal conductivity $\left(\frac{\text{W}}{\text{m°C}}\right)$

h_{conv}	convection coefficient $\left(\frac{\mathrm{W}}{\mathrm{m}^2\mathrm{°C}}\right)$	β	compress-traction coefficient
F	degradation fraction	δ	damage threshold
ϵ	emissivity	a	displacement $\left(\mathrm{m}\right)$
h	specific enthalpy $\left(\frac{\mathrm{J}}{\mathrm{kg}}\right)$	$\bar{\sigma}$	effective stress $\left(\mathrm{Pa}\right)$
q	heat flux $\left(\frac{\mathrm{W}}{\mathrm{m}^2}\right)$	$\mathbb{C}$	elastic constitutive tensor $\left(\mathrm{Pa}\right)$
w	mass flux $\left(\frac{\mathrm{kg}}{\mathrm{m}^2\mathrm{s}}\right)$	G_f	fracture energy $\left(\frac{\mathrm{J}}{\mathrm{m}^2}\right)$
$\dot{m}_{s\to g}$	mass flux rate $\left(\frac{\mathrm{kg}}{\mathrm{m}^2\mathrm{s}}\right)$	I	inertia $\left(\mathrm{m}^4\right)$
A_T	pre-exponential factor for decomposition reaction of polymer matrix $\left(\mathrm{s}^{-1}\right)$	r	normalised internal variable
		d	isotropic damage index
n_r	order of the decomposition reaction of the polymer matrix	ν	poisson ratio
		A	pre-exponential factor of the isotropic damage model
Q	energy source $\left(\frac{\mathrm{J}}{\mathrm{kg}}\right)$		
C_p	specific heat capacity $\left(\frac{\mathrm{J}}{\mathrm{kg°C}}\right)$	ε	strain
σ_β	Stefan-Boltzmann constant $\left(5.67 \cdot 10^{-8}\frac{\mathrm{W}}{\mathrm{m}^2\mathrm{°K}^4}\right)$	γ	engineering shear strain
		σ	stress $\left(\mathrm{Pa}\right)$
T	temperature $\left(\mathrm{°K}\right)$	τ	engineering shear stress $\left(\mathrm{Pa}\right)$
$\bar{T}$	prescribed temperature $\left(\mathrm{°K}\right)$	ς	stress weight factor
R	universal gas constant $\left(8.314\frac{\mathrm{J}}{\mathrm{kmol°K}}\right)$	E	Young modulus $\left(\mathrm{Pa}\right)$
θ	fibre orientation $\left(\mathrm{m}^{-1}\right)$	χ	Mourtiz and Gibson fitting parameter
l_c	characteristic length $\left(\mathrm{m}\right)$	α	thermal expansion coefficient $\left(\mathrm{°K}^{-1}\right)$

1 INTRODUCTION

Fibre Reinforced Polymers (FRP) play a major role on design of modern marine applications such as crafts with lengths below 50 m. Its use ranges from pleasure crafts, sailing boats to passenger and car ferries or patrol and rescue crafts, basically ships that are below 50m length. Nevertheless, only a few complete vessels greater than 50m have been built using composite FRP materials. This limitation is attributable to the fulfilment of what is referred to as '*steel equivalent*' structural materials in order to comply with the fire-safety requirements established by the Convention for the Safety of Life at Sea (SOLAS).

However, modern design has incorporated a wide range of techniques that with the correct use of fire retardant resins, intumescent coatings, fire insulation and fire-fighting systems extent the capabilities of FRP structures in order to comply any fire safety regulations. In fact, it is quite known that composites present a heat conduction rate lower than metals that presents a deterrent barrier against the spread of fire. The latter constitutes a well known precedent, e.g., HMS Ledbury and HMS Cattistock, which both were all-composite minehunter vessels, reported a fire scenario originated in the machinery room. HMS Cattistock reported that the fire originated in the machinery room persisted for over four hours prior to being extinguished. Both ships sustained an incredible damage of the compartments, i.e., the composite hull and bulkhead were severely charred, however the low thermal conductivity worked as a 'blockade' by stopping the fire from spreading to the neighbour compartments by heat conduction. This is generally more difficult to stop in steel shipsGibson et al. (2004).

This research relates to the H2020 project FIBRESHIP, which main objective has been to develop the knowledge and technology required to enable the building of the complete hull and superstructure of

large-length ships in composited. The marine application case presented in this paper is one of the three composite large-length vessels designed within the scope of FIBRESHIP and specifically this paper focuses on the fire-collapse analysis of the composite container ship.

Fire in composite materials is a complex chemical and thermal phenomenon where substantial degradation of the mechanical properties with the additional thermal expansion may cause failure of a FRP structure Mouritz et al. (2009) due to a reduction of its stiffness and strength. The complexity resides in the pyrolysis process that is originated by the rise of temperature and can be described as the decomposition of the matrix into derived subproducts one of the most common is gas Henderson et al. (1985). The gas then propagates through the porous media by diffusion and this produced a heat reduction due to convection.

There are different approaches in the literature on how to model the through-thickness temperature distribution, the one used in this work was proposed by Henderson et al. Henderson et al. (1985) and solves the one dimensional heat transfer equation taking into account the pyrolysis effect. Improvements of this models are introduced in Dodds et al. (2000); Gibson et al. (1995); Henderson and Wiecek (1987); Looyeh and Bettess (1998); Lua et al. (2006) and specially Chippendale et al. (2014) presents a model that couples the thermal and pyrolysis effect with the gas generation and convection of the latter through the matrix.

The thermo-mechanical analysis of laminates exposed to high temperatures has been thoroughly studied during the past two decades. Gibson et al. Gibson et al. (2004) focused on the post-fire mechanical properties of laminates and employed the concept of the two-layer mechanical model, introduced by Mouritz and Mathys, which aims to model the charring of the materialMouritz and Mathys (1999, 2000, 2001). Feih et al. studied the relationship between tensile and compressive strength and its dependency with the temperature at different heat rates Feih et al. (2006, 2007).

Composite constitutive models are a complex topic and present a wide range of solutions, the FRP laminate model assumes that the material is a unidirectional long fibre-reinforced laminate and is best described by the classical mixtures theory (CMT). The theory was further developed by Green and Naghdi Green and Naghdi (1965) and this model, namely the Rule of Mixtures (ROM), fulfils the hypothesis proposed originally by Reuss Reuss (1929) and Voigt Voigt (1889), which are a parallel or iso-strain and serial or iso-stress hypothesis respectively. The theory assumes that each material contributes to the equivalent property layer by their volume fraction and assumes an homogenised morphological distribution. The ROM is further enhanced Car et al. (2000); Rastellini et al. (2008) and Rastellini et al. in Rastellini et al. (2008) proposes the so-called Serial/Parallel Rule of Mixtures (SPROM) that deals with the orthotropy of the laminate from a constituent perspective by assuming that materials aligned with the fibre direction behave as parallel and otherwise as serial. The SPROM also accounts for non-linear analysis since it is able to keep track of the internal variables of each constituent material at layer level.

In this paper, the CFD code Fire Dynamics Simulator (FDS) Mcgrattan et al. is used to calculate the adiabatic surface temperatures of the structures in fire conditions. FDS is a large eddy simulation (LES) code for modelling incompressible, thermally-driven flows with low Mach number. The governing equations for the flow, consisting of conservation equations of mass, momentum and energy as well as the ideal gas law, are solved with a finite difference method using an explicit predictor-corrector scheme. FDS is both temporally and spatially second-order accurate. To simulate enclosure fires, FDS can be used to model, e.g., combustion, radiation, thermal degradation of solids and mechanical ventilation. Mcgrattan et al.

Hence this paper focuses on the development of a thermo-mechanical model with pyrolysis for the application of laminate composite structures under high-temperature. The model combines the one-dimensional heat model proposed by Henderson et al. together with the mechanical model based on both 3D shells and the SPROM theory from Rastellini et al. to model the composite behaviour, the

SPROM has been modified to incorporate the effect of thermal expansion. The model is implemented numerically with in-house software and coupled with a fire dynamics solver (FDS Mcgrattan et al.) in order to obtain the adiabatic temperature of the exposed and unexposed surfaces, this temperature is therefore introduced in the thermo-mechanical model as boundary conditions to estimate the heat flux. This constitutes the framework that allows the analysis of FRP structures under fire load, two verification models are presented from the literature, one for the thermal model Henderson et al. (1985) and another for the thermo-mechanical model Feih et al. (2006). Once the correctness of the implementation is demonstrated, an analysis of time-to-failure of a composite laminated structure in the presence of fire is given by using the framework explained. This last analysis is focused on the particular application of marine composite and steel structures, in special, a demonstration on how to optimally assess the fire hazard for a given fire scenario and to present a comparison between steel and composite structures, which is useful to illustrate the '*steel equivalent*' structural material concept required in SOLAS.

2 THERMAL MODEL

The thermal model combines the governing model proposed by Henderson et al. Henderson et al. (1985) and the flux boundary conditions are prescribed using the definition of adiabatic temperature introduced by Wickstrom Ulf et al. Wickstrom Ulf et al. (2007)

$$\begin{cases} \rho C_p \frac{\partial T}{\partial t} = \nabla \cdot (k \nabla T) - \mathbf{w_g} C_{p_g} \nabla T - \frac{\partial \rho}{\partial t}(Q_p + h_s - h_g) & \forall x \in \Omega, t \geq 0 \\ q = (-k \boldsymbol{\nabla} \mathbf{T}) \cdot \mathbf{n} = \left(\sigma_\beta \epsilon (\bar{T}_k^4 - T_k^4) + h_{conv}(\bar{T} - T) \right) & \forall x \text{ on } \partial\Omega, t \geq 0 \\ \rho(t=0) = \rho_0 & \forall x \in \Omega \\ T(t=0) = T_0 & \forall x \in \Omega \end{cases} \tag{1}$$

where C_p is the specific heat capacity, T is the temperature, k is the through-thickness thermal conductivity, h_g is the gas specific enthalpy, $\mathbf{w_g}$ is the gas mass flux, C_{p_g} is the gas specific heat capacity, Q_p is the polymer degradation energy source, h_s is the solid specific enthalpy, q is the normal heat flux component, $\mathbf{n}$ is the normal, σ_β is the Stefan-Boltzmann constant, ϵ is the emissivity, $T_{ad,k}$ is the adiabatic hot face temperature in Kelvin, T_{ad} is the adiabatic hot face temperature in Celsius, h_{conv} is the convection coefficient, $T_{\infty,k}$ is the ambient temperature in Kelvin, T_∞ is the ambient temperature in Celsius, Ω is the total domain and $\partial\Omega$ refers to the domain boundary.

2.1 Gas transfer model

The media is considered porous Coussy (2003) and biphasic (gas and solid).

$$\rho := \phi_s \rho_s + \phi_g \rho_g \quad , \quad \phi_i := \frac{\Omega_i}{\Omega} = \frac{\Omega_i}{\Omega_s + \Omega_g} \tag{2}$$

where ϕ_i is the phase volume fraction, ρ_0 is the virgin density , ρ_f is the char density , ρ_i is the phase volume that can be either the solid volume (ρ_s) or the gas volume (ρ_g).

Mass balance is achieved by assuming no mass flux of solid phase ($\mathbf{w_s} = 0$) and that the solid mass flux rate is equal but opposite in sign to one of the gas.

$$\frac{\partial \phi_s \rho_s}{\partial t} = -\dot{m}_{s \to g} \quad , \quad \frac{\partial \phi_g \rho_g}{\partial t} = -\nabla \cdot (\mathbf{w_g}) + \dot{m}_{s \to g} \tag{3}$$

where $\dot{m}_{s\to g}$ is the mass flux rate. From Equation 3 the gas is assumed to escape ($\partial(\phi_g\rho_g)/\partial t = 0$) in a prescribed direction ($\mathbf{w_g}(l_t, t) = 0$) from the cold to the hot end.

$$\begin{cases} \frac{\partial(w_g)}{\partial x} = \dot{m}_{s\to g} = -\frac{\partial \rho}{\partial t} \\ \\ \int_x^{l_t} \frac{\partial(w_g)}{\partial x}\,\mathrm{d}x = w_g(l_t,t) - w_g(x,t) = -\int_x^{l_t} \frac{\partial \rho}{\partial t} dx \Rightarrow w_g(x,t) = \int_x^{l_t} \frac{\partial \rho}{\partial t} dx \end{cases} \tag{4}$$

where l_t is the thickness of the composite.

2.2 Pyrolysis model

Henderson et al. define two states for the solid phase, virgin and degraded, by a linear relationship such that

$$F = \frac{\rho_s - \rho_f}{\rho_0 - \rho_f} \iff \rho_s = F\rho_0 + (1-F)\rho_f \tag{5}$$

where F is the degradation fraction. The degradation parameter (F) is selected to follow an nth Arrhenius law

$$\frac{\mathrm{d}F}{\mathrm{d}t} = -A_T\big(\frac{\rho_s - \rho_f}{\rho_0 - \rho_f}\big)^{n_r} \mathrm{e}^{-\frac{E_a}{RT}} \Rightarrow \frac{\partial \rho}{\partial t} = (\rho_0 - \rho_f)\frac{\mathrm{d}F}{\mathrm{d}t} \tag{6}$$

where A_T is the pre-exponential factor for decomposition reaction of polymer matrix, n_r is the order of the decomposition reaction of the polymer matrix, E_a is the activation energy for decomposition reaction of polymer matrix and R is the universal gas constant.

3 MECHANICAL MODEL

The mechanical composite model is the Serial/Parallel Rule of Mixture (SPROM) proposed by Rastellini et al. (2008) and extended in this work to introduce the effect of thermal expansion. The shell theory employed by this model is based on Reissner-Mindlin flat shell theory Mindlin (1989); Reissner (1945) that defines $\boldsymbol{\varepsilon} := [\varepsilon_x, \varepsilon_y, \gamma_{xy}, \gamma_{yz}, \gamma_{zx}]^T$ and $\boldsymbol{\sigma} := [\sigma_x, \sigma_y, \tau_{xy}, \tau_{yz}, \tau_{zx}]^T$ as the mechanical strain and stress vector respectively expressed in Voigt notation. A four-noded QLLL flat shell quadrilateral element has been implemented based on Oñate (2013), which combines the classical 4-noded plane stress quadrilateral matrix (Liu and Quek (2013)) and the QLLL plate element (Oñate (1994)).

3.1 Serial-parallel rules of mixing (SPROM)

The SPROM uses the notion of projector matrices in serial and parallel direction to subdivide the stress and strains in their respective parallel/serial vectors (Equation 7, Equation 8). These projections fulfil the iso-strain and iso-stress hypothesis of the conventional Rule of Mixtures (ROM) expressed in Equation 9 and Equation 10. The iso-strain hypothesis is fulfil by default since is a displacement-driven problem, the iso-stress hypothesis is fulfilled by minimising the difference between the serial stresses of the matrix and fibre phases using an iterative scheme.

$$\boldsymbol{\varepsilon} \equiv \boldsymbol{\varepsilon}_\mathbf{p} + \boldsymbol{\varepsilon}_\mathbf{s} = \mathbf{P}_{\mathbf{p},\boldsymbol{\varepsilon}}\boldsymbol{\varepsilon} + \mathbf{P}_{\mathbf{s},\boldsymbol{\varepsilon}}\boldsymbol{\varepsilon} \tag{7}$$

$$\boldsymbol{\sigma} \equiv \boldsymbol{\sigma}_\mathbf{p} + \boldsymbol{\sigma}_\mathbf{s} = \mathbf{P}_{\mathbf{p},\boldsymbol{\sigma}}\boldsymbol{\sigma} + \mathbf{P}_{\mathbf{s},\boldsymbol{\sigma}}\boldsymbol{\sigma} \tag{8}$$

$$\text{Parallel} \quad \begin{cases} \boldsymbol{\varepsilon}_\mathbf{p} = \boldsymbol{\varepsilon}_{\mathbf{p,f}} = \boldsymbol{\varepsilon}_{\mathbf{p,m}} \\ \boldsymbol{\sigma}_\mathbf{p} = \phi_f\boldsymbol{\sigma}_{\mathbf{p,f}} + \phi_m\boldsymbol{\sigma}_{\mathbf{p,m}} \end{cases} \tag{9}$$

$$\text{Serial} \quad \begin{cases} \boldsymbol{\sigma}_\mathbf{s} = \boldsymbol{\sigma}_{\mathbf{s,f}} = \boldsymbol{\sigma}_{\mathbf{s,m}} \\ \boldsymbol{\varepsilon}_\mathbf{s} = \phi_f\boldsymbol{\varepsilon}_{\mathbf{p,f}} + \phi_m\boldsymbol{\varepsilon}_{\mathbf{p,m}} \end{cases} \tag{10}$$

where $\boldsymbol{\sigma_{p,m}}$ is the parallel matrix stress, $\boldsymbol{\sigma_{s,m}}$ is the serial matrix stress, $\boldsymbol{\sigma_{p,f}}$ is the parallel fibre stress, $\boldsymbol{\sigma_{s,f}}$ is the serial fibre stress, $\boldsymbol{\sigma_{s}}$ is the serial composite stress, $\boldsymbol{\sigma_{p}}$ is the parallel composite stress, $\boldsymbol{\varepsilon_{p,m}}$ is the parallel matrix strain, $\boldsymbol{\varepsilon_{s,m}}$ is the serial matrix strain, $\boldsymbol{\varepsilon_{p,f}}$ is the parallel fibre strain, $\boldsymbol{\varepsilon_{s,f}}$ is the serial fibre strain, $\boldsymbol{\phi_{m}}$ is the matrix volume fraction and $\boldsymbol{\phi_{f}}$ is the fibre volume fraction.

3.2 Thermal constitutive model of the constituent materials

Each constituent material that is part of the composite is modelled using the isotropic damage model described in Chaves (2013). Assume that each constituent material (fibre and matrix) can be represented by the notation 'i', the isotropic constitutive damage model yields

$$\boldsymbol{\sigma_i} := (1 - d_i)\mathbb{C}_\mathbf{i}(\boldsymbol{\varepsilon_i} - \boldsymbol{\varepsilon_{T,i}}), \quad \forall i \in f, m \tag{11}$$

where σ_i is the stress, ε_i is the strain, d_i is the isotropic damage index, $\mathbb{C}_i$ is the elastic constitutive tensor and $\varepsilon_{T,i}$ is the thermal strain for the constituent material 'i' (fibre or matrix). The thermal strain of each of the constituent materials is anisotropic

$$\boldsymbol{\varepsilon_{T,i}} := \boldsymbol{\alpha_i}\Delta T = \boldsymbol{\alpha_i}\big(T(x,t) - T(x,0)\big), \quad \forall i \in f, m \tag{12}$$

where α_i is the thermal expansion coefficient and is defined as $\boldsymbol{\alpha} := [\alpha_x, \alpha_y, 0, 0, 0]^T$.

Note that the Young modulus (E) and the yield stress (σ_y) depends both on the temperature (T) and the formation of pyrolysis (F) Mouritz and Gibson (2006).

$$P_i(T,F) = \left(\frac{P_{u,i} + P_{r,i}}{2} - \frac{P_{u,i} - P_{r,i}}{2}\tanh\chi_{1,i}(T - T_{g,i})F^{\chi_{2,i}}\right), \quad \forall i \in f, m \tag{13}$$

where (P_u) is the unrelaxed and (P_r) is the relaxed value of a generic property (P), $T_{g,i}$ is the glass transition temperature, $\chi_{1,i}$ is the first Mourtiz and Gibson fitting parameter, $\chi_{2,i}$ is the second Mourtiz and Gibson fitting parameter.

The developed damage criteria for the yielding surface Chaves (2013) has to be adapted to take into account the effects of the temperature. This necessarily modifies the yielding surface threshold, e.g., the stress norm and the damage exponential evolution law have to fulfil the following equalities

$$\begin{cases} \delta_i = \left(\varsigma + \dfrac{1-\varsigma}{\beta_i}\right)\sqrt{E_{0,i}}\sqrt{\dfrac{\bar{\boldsymbol{\sigma}}_\mathbf{i}}{\sigma_{y,i}} : (\mathbb{C}_{\mathbf{0,i}})^{-1} : \dfrac{\bar{\boldsymbol{\sigma}}_\mathbf{i}}{\sigma_{y,i}}} & \forall i \in f, m \\ A_i = \left(\dfrac{G_{f_i}E_i}{l_{c,i}\,\sigma_{y,i}^2} - \dfrac{1}{2}\right) \rightarrow \dfrac{G_{f_i}E_i}{\sigma_{y,i}^2} = \text{constant} & \forall i \in f, m \end{cases} \tag{14}$$

where $\bar{\sigma}_i$ is the effective stress, δ_i is the damage threshold, ς is the stress weight factor, $\beta_{,i}$ is the compress-traction coefficient, $E_{0,i}$ is the initial Young modulus, $\sigma_{y,i}$ is the yield stress, which is considered to be dependent of the temperature and the degradation factor, $\mathbb{C}_{0,i}$ is the initial elastic constitutive tensor, $A_{,i}$ is the pre-exponential factor of the isotropic damage model , $l_{c,i}$ is the characteristic length and G_{f_i} is the fracture energy. In broad terms, Equation 14, adds the temperature effect from Equation 13 and states that if the yielding stress varies, generally speaking negative monotic variation, the yielding threshold is reduced and thus the damage increased due to thermal degradation. Another key assumption is to set the pre-exponential mechanical factor (A_i) constant respect to the temperature.

3.3 SPROM with thermal expansion

In this section, the theory detailed in Rastellini et al. (2008) has been modified to include the thermal expansion effect. Equation 11 can be expressed in differential form and projected to serial/parallel directions such as

$$\begin{array}{l} \mathrm{d}\boldsymbol{\sigma}_{\mathbf{f}} := \mathbb{C}_{\mathbf{tan,m}}(\,\mathrm{d}\boldsymbol{\varepsilon}_{\mathbf{f}} - \,\mathrm{d}\boldsymbol{\varepsilon}_{\mathbf{T,f}}) \\ \mathrm{d}\boldsymbol{\sigma}_{\mathbf{m}} := \mathbb{C}_{\mathbf{tan,f}}(\,\mathrm{d}\boldsymbol{\varepsilon}_{\mathbf{m}} - \,\mathrm{d}\boldsymbol{\varepsilon}_{\mathbf{T,m}}) \end{array} \tag{15}$$

$$\mathrm{d}\boldsymbol{\sigma}_{\mathbf{p,i}} := \mathbb{C}_{\mathbf{pp,i}}(\,\mathrm{d}\boldsymbol{\varepsilon}_{\mathbf{p,i}} - \,\mathrm{d}\boldsymbol{\varepsilon}_{\mathbf{T,p,i}}) + \mathbb{C}_{\mathbf{ps,i}}(\,\mathrm{d}\boldsymbol{\varepsilon}_{\mathbf{s,i}} - \,\mathrm{d}\boldsymbol{\varepsilon}_{\mathbf{T,s,i}}), \quad \forall i \in f, m \tag{16}$$

$$\mathrm{d}\boldsymbol{\sigma}_{\mathbf{s,i}} := \mathbb{C}_{\mathbf{sp,i}}(\,\mathrm{d}\boldsymbol{\varepsilon}_{\mathbf{p,i}} - \,\mathrm{d}\boldsymbol{\varepsilon}_{\mathbf{T,p,i}}) + \mathbb{C}_{\mathbf{ss,i}}(\,\mathrm{d}\boldsymbol{\varepsilon}_{\mathbf{s,i}} - \,\mathrm{d}\boldsymbol{\varepsilon}_{\mathbf{T,s,i}}), \quad \forall i \in f, m \tag{17}$$

where

$$\mathbb{C}_{\mathbf{tan,i}} := \begin{bmatrix} \mathbb{C}_{\mathbf{pp,i}} & \mathbb{C}_{\mathbf{ps,i}} \\ \mathbb{C}_{\mathbf{sp,i}} & \mathbb{C}_{\mathbf{ss,i}} \end{bmatrix} \equiv \begin{bmatrix} \dfrac{\partial \boldsymbol{\sigma}_{\mathbf{p,i}}}{\partial \boldsymbol{\varepsilon}_{\mathbf{p,i}}} & \dfrac{\partial \boldsymbol{\sigma}_{\mathbf{p,i}}}{\partial \boldsymbol{\varepsilon}_{\mathbf{s,i}}} \\ \dfrac{\partial \boldsymbol{\sigma}_{\mathbf{s,i}}}{\partial \boldsymbol{\varepsilon}_{\mathbf{p,i}}} & \dfrac{\partial \boldsymbol{\sigma}_{\mathbf{s,i}}}{\partial \boldsymbol{\varepsilon}_{\mathbf{s,i}}} \end{bmatrix} \equiv \begin{bmatrix} \mathbf{P}_{\mathbf{p},\boldsymbol{\sigma}} \mathbb{C}_{\mathbf{tan,i}} \mathbf{P}_{\mathbf{p},\boldsymbol{\varepsilon}} & \mathbf{P}_{\mathbf{p},\boldsymbol{\sigma}} \mathbb{C}_{\mathbf{tan,i}} \mathbf{P}_{\mathbf{s},\boldsymbol{\varepsilon}} \\ \mathbf{P}_{\mathbf{s},\boldsymbol{\sigma}} \mathbb{C}_{\mathbf{tan,i}} \mathbf{P}_{\mathbf{p},\boldsymbol{\varepsilon}} & \mathbf{P}_{\mathbf{s},\boldsymbol{\sigma}} \mathbb{C}_{\mathbf{tan,i}} \mathbf{P}_{\mathbf{s},\boldsymbol{\varepsilon}} \end{bmatrix}, \quad \forall i \in f, m \tag{18}$$

$\mathbb{C}_{\mathbf{tan,m}}$ is the matrix tangent elastic constitutive tensor and $\mathbb{C}_{\mathbf{tan,f}}$ is the fibre tangent elastic constitutive tensor.

The SPROM defines the serial matrix strain as an internal variable such that it fulfils the iso-stress hypothesis. The serial matrix strain can be defined in an incremental manner and use a Newton-Raphson scheme to obtain the optimal serial increment of the matrix strain in order to fulfil the iso-stress hypothesis. The initial prediction ($k = 0$) is based on the converged serial matrix strain of the previous converged step. Being

$$\boldsymbol{\varepsilon}_{\mathbf{s,m}}(t + \Delta t)|_0 = \boldsymbol{\varepsilon}_{\mathbf{s,m}}(t)|_0 + \boldsymbol{\Delta\varepsilon}_{\mathbf{s,m}}|_0 \tag{19}$$

The initial prediction can be obtained by assuming that in Equation 17 the serial incremental internal stress is the same for both matrix and fibre

$$\begin{array}{c} \boldsymbol{\Delta\sigma}_{\mathbf{s,m}} = \boldsymbol{\Delta\sigma}_{\mathbf{s,f}} \\ \Downarrow \\ \mathbb{C}_{\mathbf{sp,m}}(\boldsymbol{\Delta\varepsilon}_{\mathbf{p,m}} - \boldsymbol{\Delta\varepsilon}_{\mathbf{T,p,m}}) + \mathbb{C}_{\mathbf{ss,m}}(\boldsymbol{\Delta\varepsilon}_{\mathbf{s,m}} - \boldsymbol{\Delta\varepsilon}_{\mathbf{T,s,m}}) = \\ \mathbb{C}_{\mathbf{sp,f}}(\boldsymbol{\Delta\varepsilon}_{\mathbf{p,f}} - \boldsymbol{\Delta\varepsilon}_{\mathbf{T,p,f}}) + \mathbb{C}_{\mathbf{ss,f}}(\boldsymbol{\Delta\varepsilon}_{\mathbf{s,f}} - \boldsymbol{\Delta\varepsilon}_{\mathbf{T,s,f}}) \end{array} \tag{20}$$

By substituting Equation 16 in Equation 20 and also exchanging the incremental serial strain of the fibre as defined in Rastellini et al. (2008), the initial prediction yields

$$\boldsymbol{\Delta\varepsilon}_{\mathbf{s,m}}|_0 = \mathbb{M} : \Big(\mathbb{C}_{\mathbf{sp,m}} \boldsymbol{\Delta\varepsilon}_{\mathbf{s}} + \phi_f (\mathbb{C}_{\mathbf{sp,f}} - \mathbb{C}_{\mathbf{sp,m}}) \boldsymbol{\Delta\varepsilon}_{\mathbf{p}} + \phi_f \boldsymbol{\Delta\sigma}_{\mathbf{T,m}} - \phi_f \boldsymbol{\Delta\sigma}_{\mathbf{T,f}} \Big) \tag{21}$$

$$\mathbb{M} = \Big(\phi_f \mathbb{C}_{\mathbf{ss,m}} + \phi_m \mathbb{C}_{\mathbf{ss,f}}\Big)^{-1} \tag{22}$$

$$\boldsymbol{\Delta\sigma}_{\mathbf{T,m}} = \mathbb{C}_{\mathbf{sp,m}} \boldsymbol{\Delta\varepsilon}_{\mathbf{T,p,m}} + \mathbb{C}_{\mathbf{ss,m}} \boldsymbol{\Delta\varepsilon}_{\mathbf{T,s,m}} \tag{23}$$

$$\boldsymbol{\Delta\sigma}_{\mathbf{T,f}} = \mathbb{C}_{\mathbf{sp,f}} \boldsymbol{\Delta\varepsilon}_{\mathbf{T,p,f}} + \mathbb{C}_{\mathbf{ss,f}} \boldsymbol{\Delta\varepsilon}_{\mathbf{T,s,f}} \tag{24}$$

where $\Delta\ \sigma_{T,f}$ is the incremental stress of the fibre and $\Delta\ \sigma_{T,m}$ is the incremental stress of the matrix due to thermal expansion. Both terms are the result of extending the regular SPROM in Rastellini et al. (2008) in order to take into account the effect of deformation under elevated temperatures.

4 VALIDATION OF THE NUMERICAL MODEL

4.1 Thermal Model - Henderson experimental test

The thermal model developed in this work, which is based on the model proposed by Henderson et al. and that solves the one dimensional heat transfer equation with pyrolysis for non-homogeneous materials (composites), is tested against the experimental data provided by the same author. The experimental data presented by Henderson et al. in Henderson et al. (1985) will be used. The material employed in these tests was a laminated stack composed of phenolic resin, glass fibre and talc as filler. The volumetric fibre fraction of the glass fibre is $\phi_f = 60.5\%$ and the specimens of cylindrical shape are defined by 1cm of diameter and 3cm of height. The specimens were exposed to a high radiant heat flux source of 279.7kW/m^2 and four thermocouples were inserted at depths of 0.1, 0.5, 1.0 and 2.9cm from the exposed surface in order to monitor the temperatureHenderson and Hagen (1985).

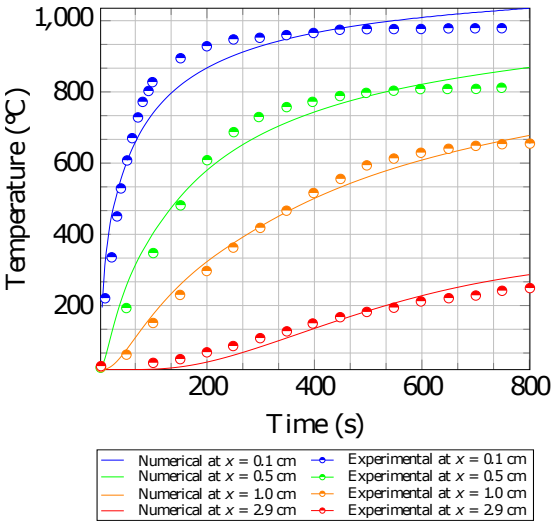

Figure 1: Evolution of the temperature ($T(x,t)$) of the experimental and numerical results at different thickness positions.

In Figure 1, the numerical temporal evolution of the temperature at different positions of the thickness is compared against the experimental data. The agreement of the numerical and experimental data is excellent. Only a tiny difference is shown during the transient and for those thermocouples situated near the exposed surface.

4.2 Thermo-mechanical Model - Feih experimental test

For the thermo-mechanical implementation, the numerical results are compared against the experiments of Feih et al. (2006), in particular the experimental data provided for the compression test. In Feih et al. (2006), the thermal properties are setup as described in the paper, the calibration is based on TGA, DMTA and DSC analyses. The standard manner to prescribe the boundary conditions is to prescribe a numerical constant heat flux, in this work, the concept of adiabatic temperature is employed instead Wickstrom Ulf et al. (2007). The adiabatic temperature is calculated based on the hot surface temperature Equation 1 assuming a prescribed constant heat flux at each time step for free convection by taking into account that the convection coefficient depends on the heat flux and also in the difference of temperature between the adiabatic and exposed temperatures. The choice of thermal degradation properties is the same as in the literature and the numerical model predicts well the experimental results in Figure 2.

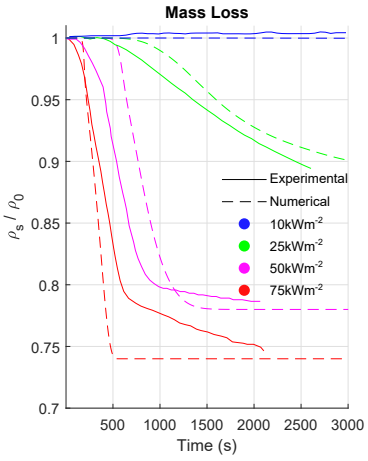

Figure 2: Comparison of numerical and experimental remaining mass evolution respect to the time for different heat flux loads.

The thermal model is then compared against the experimental tests of an specimen exposed to high temperatures, this experiment aims to generate a temperature profile through the thickness of the specimen by applying a constant heat flux.

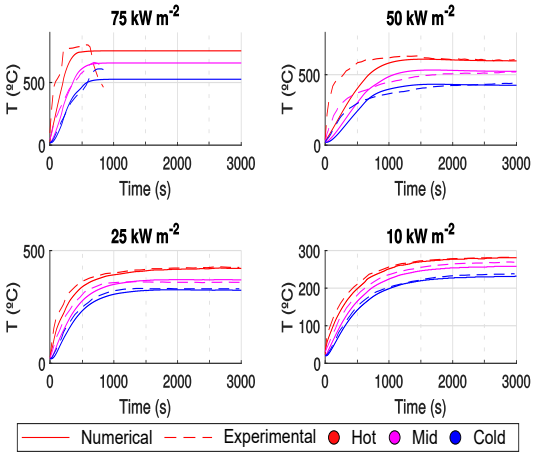

Figure 3: Experimental and numerical thermocouple readings at different positions through-thickness (Cold = 0 mm, Mid = 4.5 mm and Hot = 9 mm) and different heat fluxes.

Figure 3 shows the evolution of the experimental data measured by the thermocouples located at the cold, mild and hot layers at 0, 4.5 and 9mm respectively. The evolution of the temperature respect to time is almost identical for heat flux loads of 10 and 25 kW/m^2. The main discrepancies are again for higher heat fluxes, e.g., the 50 kW/m^2 case shows a good steady solution however the transient presents a steeper evolution in the experimental test. This difference is mentioned in the original paper Feih et al. (2006) and it is attributed to the escape of the gas through the thermocouples and even the numerical solutions provided by Feih do not match with the experimental ones. The special case of 75 kW/m^2 is also reproduced despite the fact that the hot end ignites. In the numerical simulation, it has been considered what would happen if the temperature remains the maximum instead of decaying in order to maintain the heat flux constant. The numerical results that Feih provides for this case match perfectly at the beginning and then diverge significantly, the results provided in this work match for a wider range of time specially for the cold and mid curves, however the hot slope is lower compared to the experimental data.

The thermo-mechanical model is validated against the compression tests results. These tests evaluate the compression endurance of the specimens, which are prone to buckling rather than yielding, when exposed to high temperatures. The main objective is to infer a relationship between yield failure and temperature. Feih employs Equation 13 to establish a relationship between the yielding stress and the temperature then loads the specimens for different values below of the buckling load at ambient temperature. According to Feih, the specimens are constraint in such manner that avoids global buckling, therefore the specimens shall only fail by a yielding as the temperature rises and the yielding stress is reduced.

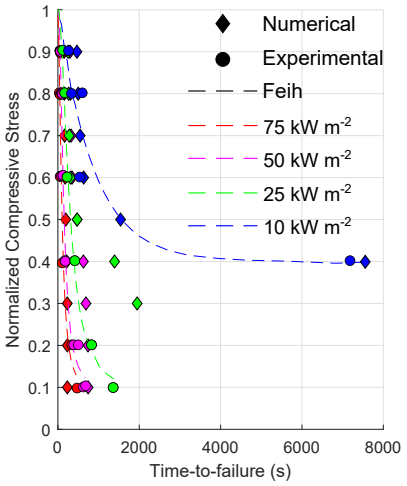

Figure 4: Thermo-mechanical failure of the compression specimens for a combination of different thermal and mechanical loads.

The compression failure of the specimens is then summarised and detailed in Figure 4. The experimental and the numerical results provided by the thermo-mechanical model match for the heat flux of 10 kW/m^2 and present a close agreement for 50 and 75 kW/m^2. In the other hand, the case of 25 kW/m^2 shows an initial good agreement but as the load is decreased, lower or equal to a 30% of the buckling load ambient temperature, the numerical and experimental solutions diverge. One of the reasons for this mismatch may be due to the neglect of the Young's modulus degradation, since the degradation of this property leads to a lower flexural rigidity (EI) which is linearly related to the buckling load. Since the thermo-mechanical analysis presented in this article focuses on linear geometric kinematics, this final remark cannot be checked.

5 FIRE RESISTING MARINE FRP DIVISIONS ANALYSIS

The fire collapse analysis of an area of the superstructure of a containership is presented in this section. In this particular case, non-structural resistant members located on one of the decks of the superstructure were analysed. In the scenario studied, the fire starts in the laundry via the ignition

of the different cloths hanging on the towel rack.

Two fire scenarios were considered, closed doors and open doors. All doors are considered closed and thus the ventilation between rooms is significantly reduced, the opposite case is where the door that connects the laundry and corridor 1 is open and the door that connects corridor 1 and the outside room is open as well. By analysing these two possible scenarios, the effect and role that ventilation has during fire propagation is taken into account. Each one of these fire scenarios is simulated for Steel and FRP divisions, the first considers no pyrolysis and the second considers a laminate composed of layers of glass fibre($\phi = 55\%$) and vinylester resin, the stacking information can be found in Figure 5b. All the materials are covered with an external layer of insulation. The mechanical load applied to the ceiling of the structure is considered as per regulations requirement, DNV 201 (2016) recommends a design pressure load of 350 N/m^2 in the superstructure.

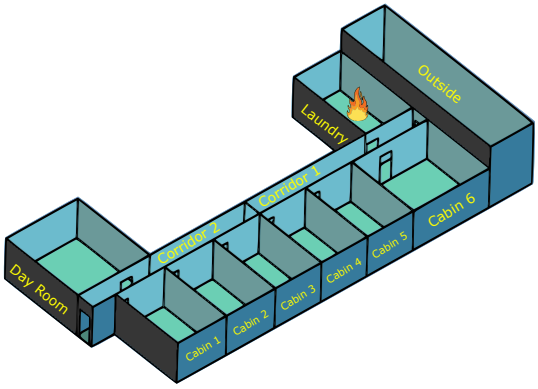

(a) Domain of the fire scenario.

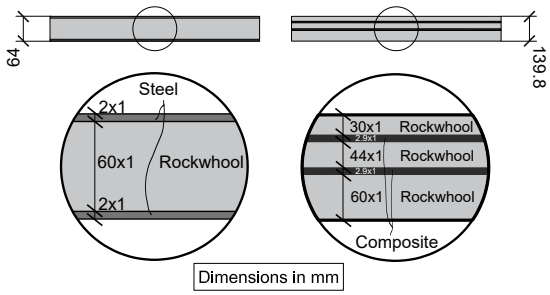

(b) Thickness stacking of the divisions.

Figure 5: Thermo-mechanical analysis of the superstructure of a containership.

The computational model of the domain in Figure 5a was discretised in a finite mesh of 671680 hexahedra elements with an element size of 10cm for the fire-CFD solver, the simulation time is 1 hour and the time stepping is 0.1 seconds. The resultant adiabatic temperature from the CFD is interpolated into the thermo-mechanical mesh that is an unstructured quadrilateral mesh of 23564 QLLL elements with a maximum element size of 20cm. The through-thickness mesh of 1D linear elements of the domain in Figure 5b is divided in 14 and 19 divisions for steel and FRP panels respectively. The thermo-mechanical time scheme is fractioned in steps of 50 seconds.

The software used to undertake the fire dynamics is the Fire Dynamics Simulator (FDS) Mcgrattan et al.. The gas temperature 2 metres above the deck 15, 30, 45 and 60 minutes after the fire ignition is shown for each studied scenario in Figure 6. The effect of ventilation can be clearly seen in the figures, as the simulations with two open doors have higher maximum temperatures as there is more oxygen available for combustion. In the simulations with FRP divisions, the temperatures are higher than in the simulations with steel divisions, as the combustible divisions participate in the fire. The difference is significant especially in the scenarios with two open doors, as the fire spreads to corridor bulkheads in the simulation with FRP.

Soot concentration 2 metres above the deck 15, 30, 45 and 60 minutes after the fire ignition is shown for each studied scenario in Figure 7. During the fire, the laundry room and the corridor are most affected by the smoke in all studied scenarios, but all rooms receive some smoke during the simulations due to the pressure differences. In the simulations with steel divisions, two open doors lead to more effective ventilation of smoke. It can be seen that the burning FRP materials produce significant amount of smoke, leading to higher soot concentrations for longer time.

FDS is used to obtain the adiabatic temperature that is later introduced as thermal boundary conditions in the thermo-mechanical problem. The thermal loads are divided in four regions: *laundry, corridor 1, corridor 2 and other rooms* and the resultant adiabatic temperature of those can be found in **??** for the four combination scenarios (open/closed doors and steel/FRP material). Note that the

other rooms temperature is considered as the ambient temperature (approximately 20°C).

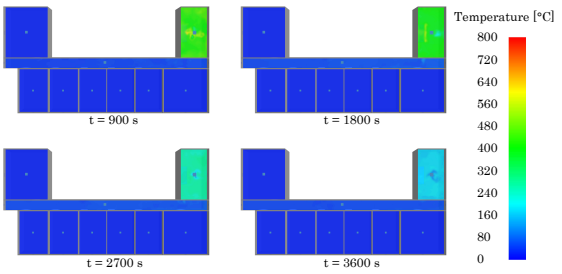

(a) Steel structures, doors closed

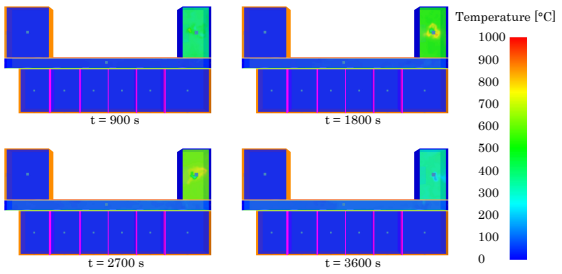

(b) FRP structures, doors closed

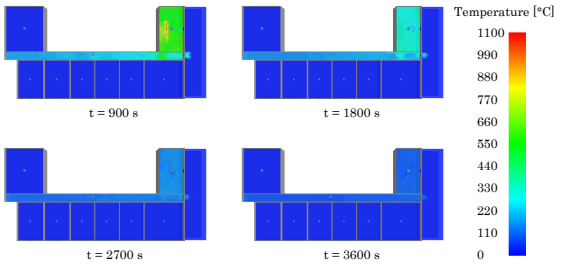

(c) Steel structures, two open doors

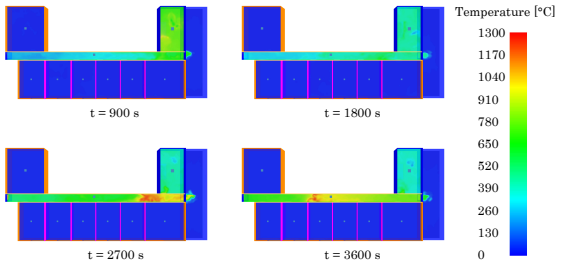

(d) FRP structures, two open doors

Figure 6: Gas temperature 2.0 metres above the deck 15, 30, 45 and 60 minutes after the fire ignition in each studied scenario.

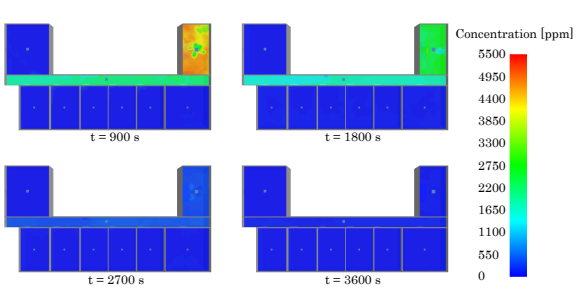

(a) Steel structures, doors closed

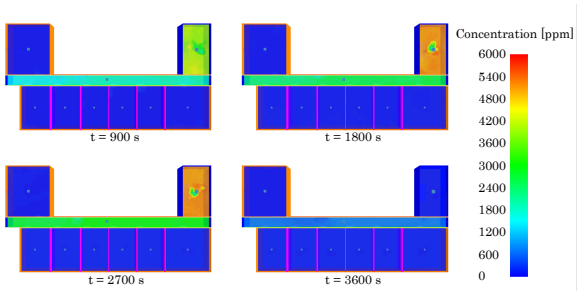

(b) FRP structures, doors closed

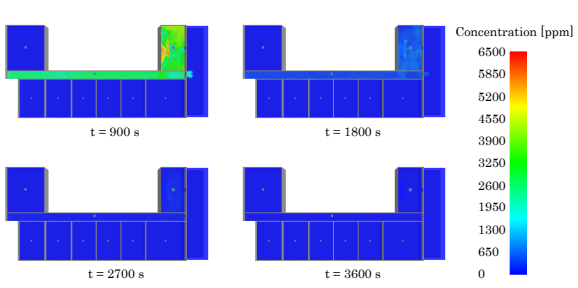

(c) Steel structures, two open doors

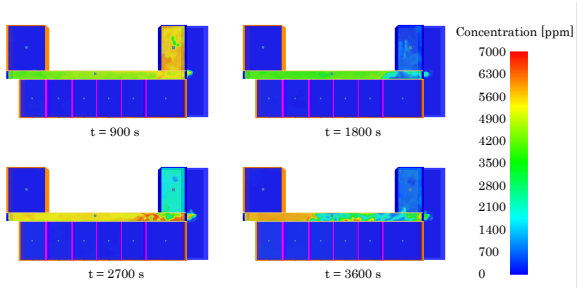

(d) FRP structures, two open doors

Figure 7: Soot concentration 2.0 metres above the deck 15, 30, 45 and 60 minutes after the fire ignition in each studied scenario.

The four different case scenarios can be described in the following manner:

- Steel - closed doors:

  The doors are shut, therefore the ventilation and O_2 renovation is limited. The *laundry* temperature increases rapidly up to a maximum temperature of 450°C around 1500s, then the room is depleted of oxygen and the fire starts to auto-extinguish in an slow but monotonic manner. The temperature in *corridor 1 and 2* raises up to 50°C around 1500s and remains steady.

- Steel - open doors: The doors that connect to the outside room are open, therefore an important apportion of O_2 is introduced in the combustion. The *laundry* temperature increases rapidly up to a maximum temperature of 600°C around 500s, then the room temperature steadily decreases to 80°C at the end of the analysis. The temperature in *corridor 1 and 2* raises up to 150°C around 500s, remains steady up to 2000s, then decreases to 60°C at the end of the analysis.

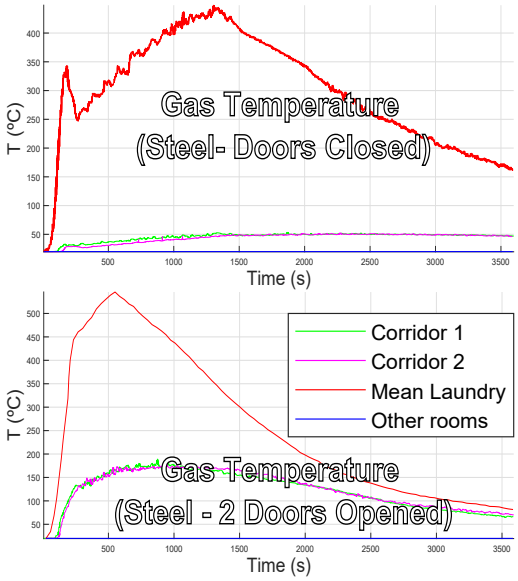

Figure 8: Thermal boundary loads for different fire scenarios. Steel.

- FRP - closed doors: The doors are shut, therefore the ventilation and O_2 renovation is limited. The *laundry* temperature increases rapidly up to a maximum temperature of 600°C around 3000s, after the temperature decreases until it reaches the value of 300°C at time 3600s. The temperature in *corridor 1 and 2* raises up to 100°C around 3000s and remains steady until the end.

- FRP - open doors: The doors that connect to the outside room are open, therefore an important apportion of O_2 is introduced in the combustion together with the pyrolysis of the material that increases the porosity of the material. The *laundry* temperature increases up to a maximum temperature of 800°C around 1300s, then the room temperature steadily decreases to 300°C at time 2500s, increases shortly to 400°C and decreases to 350°C at the end of the analysis. The temperature in *corridor 1 and 2* raises up to 300°C around 1000s, remains steady up to 1700s, then *corridor 1* slowly increases to 600°C and *corridor 2* dramatically increases to a peak of 1000°C and falls to 800°C at the end of the simulation.

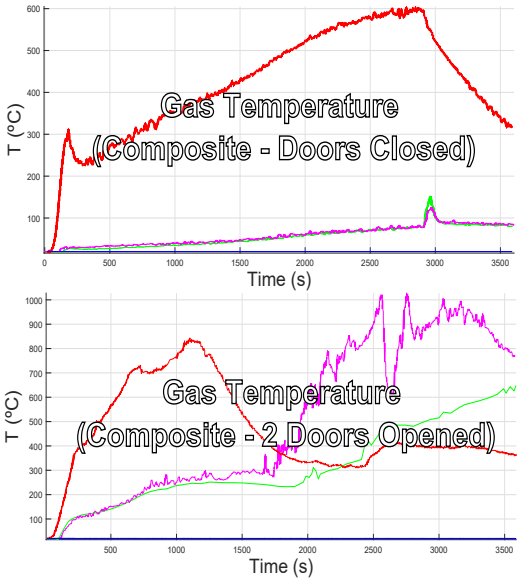

Figure 9: Thermal boundary loads for different fire scenarios. FRP.

The accumulated damage of the structure varies as the degradation of mechanical properties developes, note that the Young's modulus and the yielding stress depends on the temperature and the degradation fraction (F) according to Equation 13. The steel divisions are useful to understand that a structure can collapse only due to thermal effects. This is explained by the fact that the yielding stress reduces when the temperature increases. This is very important since many real naval applications are designed to support fixed loads – in this case the ceiling pressure – and this load is unaffected by the temperature and thus the damage will originate as the temperature rises, only due to the effective reduction of the yielding surface of the characteristic material. Otherwise, the FRP divisions will sustain damage that may originate not only due to thermal effect, but pyrolysis itself.

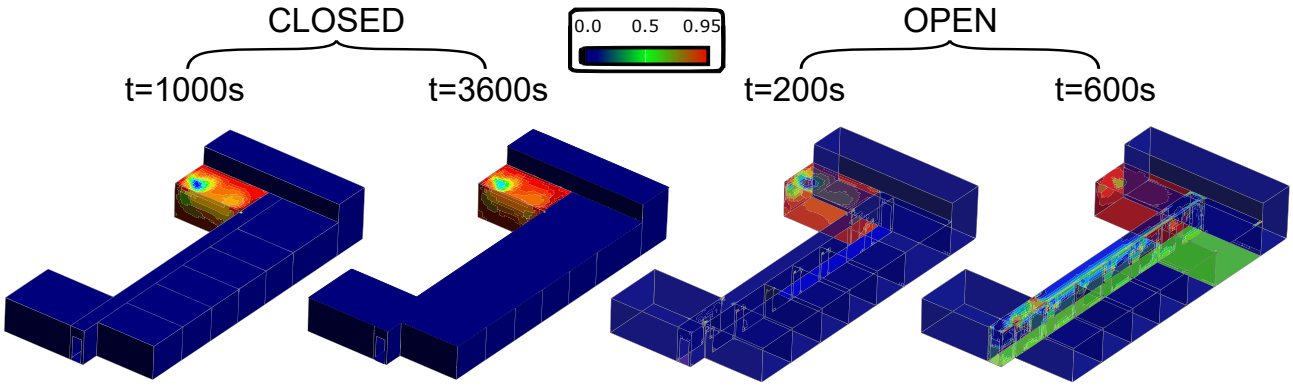

Figure 10: Damage distribution for steel material.

The response in Figure 10, when doors are closed, is in agreement with the heat originated by the adiabatic temperature. Damage is temperature-driven only and it originates early on the simulation (1000s), once the temperature in the *laundry* reaches its maximum, the damage distribution remains undisturbed until the end (3600s).

In the case of open doors in Figure 10 the damage originates earlier than in the closed doors case (200s). This is attributively to the extra ventilation, ventilation plays an important role not only on how quick the temperature rises but also the spread of combustion to other rooms as it can bee seen that both *corridor 1 and 2* have small patches of elements with a moderate damage. Once the temperature in the *laundry* reaches its maximum (600s), the damage distribution remains undisturbed until the end (3600s), however the mechanical response is increased as the temperature decreases (the structure again becomes stiffer). This can be observed in Figure 11 where the norm of the displacement decreases after arriving to the time step 1000s, this is due to the recovery of the Young's modulus as the temperature of the different regions decreases. This is interesting since it shows the mechanical post-fire response of the structure for elements that have not collapse due to the reduction of the yielding limit, however it is important to understand that while the mechanical properties have recovered, the damage does not heal.

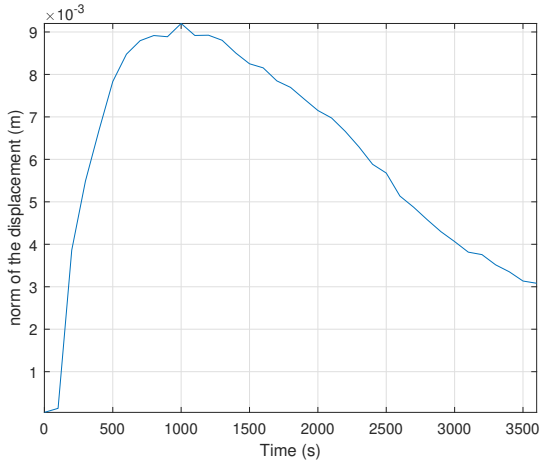

Figure 11: Deflection of a damaged element in *corridor 2*.

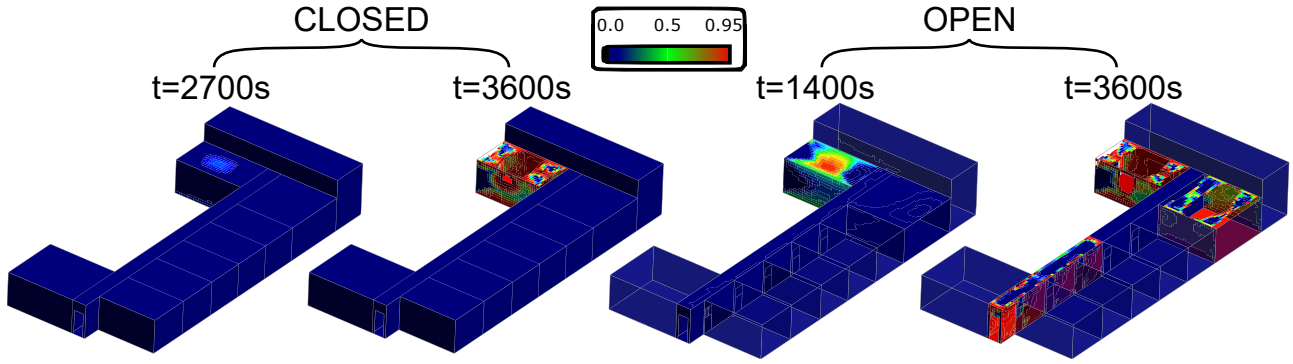

Figure 12: Damage distribution for FRP material.

Again, Figure 12, when doors are closed, reproduces a damage pattern that is in accordance to the thermal loads introduced. In this case the damage is both temperature-driven and pyrolysis-driven. The damage on the structure, compared to its steel equivalent case, is produced significantly later

on the time analysis (note that the temperature increases slower for the FRP design than the steel). Nevertheless, the sustained damage in the *laundry* room is higher than the steel for the same time of simulation, as it clearly involves not only temperature but the damaged originated due to the pyrolysis of the composite layers closed to the exposed surfaces. The overall result is that a vast region of the ceiling in the *laundry* room has degraded and no longer endures the load, reaching a point where the ceiling collapses, the collapse development is very sudden since from the origination of the damage (2700s) to the collapse (3600) there is less than 1000 seconds. On the other hand, Figure 12, when doors are open, the sustained damage on the structure is greater than the case where the doors are shut, this is obvious because there is more ventilation and therefore more combustion and spreading. The damage starts to be noticeable at 1400s that is when the temperature in the *laundry* room reaches its peak. Since the temperatures of all regions present similar or higher values to the closed doors case, analogously the *laundry* rooms collapses in this case scenario as well. However, the major problem in this case, where spreading of the fire is present, is not only the collapse of the *laundry*. Since the fire spreads, the temperature on the *corridor 1 and 2* is greater than before, even surpassing the values of 1000°C on *corridor 2* and it reaches the final simulation with the partial collapse of the ceiling of the *cabin 6*, which poses an important risk for the safety of the crew, and also the deterioration of the divisions located in the *corridor 2*, which may block the exit of the crew located on *cabin 1,2 and 3* or on the *day room*.

6 CONCLUSION

The numerical model presented in this work has shown excellent agreement reproducing the experimental data provided by both (Henderson et al., 1985) and (Feih et al., 2006). The thermal model is particularly good matching the experimental data and the thermo-mechanical model is quite accurate with some minor differences. The marine application case, the fire collapse of the divisions located in the superstructure of a containership, was used to demonstrate the correctness of a unique tool used to aid in the design of both steel and specially FRP structures. Specially the proposed framework, which couples fire dynamics and thermo-mechanical response, is a very useful tool in order to comply with the concept of '*steel equivalent*' material design that is required in many fire-safety requirements (SOLAS).

It is very interesting to compare the traditional steel design versus the modern composite design. Dividing the analysis in three categories: *thermal, mechanical, thermo-mechanical* helps understand the major differences. The key aspects when it comes to *thermal* differences in design would be first the conductivity coefficient that is it significantly greater on metals than composites, this can be observed in how temperature in the *laundry* rises significantly quicker for steel than composites. This certainly is an issue and poses several constraints for metal structure design because the time span available to control the fire or evacuate is significantly reduced. On the other hand, composites conduct slower the heat originated from fire and therefore give extra time to control the hazard, however pyrolysis might be originated during the fire dynamics process, which generally plays a greater role in the collapse of structures than temperature itself. Also composites attain, at a slower pace, maximum temperatures that are significantly higher than metals. The overall thermal design of composites is furthermore complex than metals and has to be carefully design in order to avoid major design flaws, however if performed correctly, it can grant better results specifically on delaying the collapse of the structure which is a very interesting point in this research.

The mechanical comparison is more complex since metals and composite behave significantly different. Metals are generally isotropic, which simplifies the amount of data needed to numerically model the structure, whilst composites (FRP) are clearly orthotropic. Composites are widely use in marine applications, not only because they are good at resisting corrosion, but since their strength and density ratio is significantly greater than those present on metals, that is one of the most fundamental

advantages, specially on a containership which its main requirement is to transport cargo. Indeed the difference of this ratio grants to large length composite ships the possibility to carry up to 20% more cargo than traditional solutions. Another advantage is the possibility to obtain tailored solutions by deciding the materials and layer orientations in order to reinforce structural elements optimally. Nevertheless, numerical solutions for composites are generally computational costly or experimental complex and expensive when it comes to calibration of the mechanical properties and even when numerical calibration is feasible, the solution is generally limited to linear analysis. It is with this regard that the theory used here is the so-called SPROM that acts as a constituent material manager where the materials are introduced separately and in an isotropic manner. The theory is able to extract the orthotropy of each ply in the stack and in addition, this composite constitutive theory, allows to extent the whole calculus to the non-linear range which is essential in order to assess fire-collapse.

Finally, the thermo-mechanical analysis of steel structures is simpler since pyrolysis is not produced and therefore the collapse is only due to thermal degradation of the mechanical properties as shown in the steel examples. On the other hand, when using composites as designing material, pyrolysis plays a major role and has a greater impact on the structure since both FRP divisions presented a greater damage distribution on the superstructure. There is various aspects that may exacerbate the collapse on the FRP divisions, first it is well known that the glass transition temperature of the resin is significantly lower than the steel, which will have a major impact, one by generating more pores inside the structure and second by decreasing drastically the mechanical properties (Young's modulus and yield stress). Another aspect is the char generation that is an irreversible process, in the case of the steel note that once after the fire was extinguished the deflection sustained on the ceiling was significantly decreased (one third of the deflection at maximum temperature) and this is motivated by the idea that metal do not pyrolyse whilst composite generate char and thus when the temperature decreases there is an irreversible process that yields, e.g., a lower Young's modulus after pyrolysis, for the same temperature. The last is very characteristic on post-fire scenarios and was the main objective to demonstrate in this work, which ultimately has served to provide a reliable framework in the design of large composite marine applications that may be subjected to fire (one the most important hazards in composite structures).

7 ACKNOWLEDGEMENT

This work was funded thanks to H2020 project FIBRESHIP sponsored by the EUROPEAN COMMISSION under the grant agreement 723360 "Engineering, production and life-cycle management for complete construction of large-length FIBRE-based SHIPs". www.fibreship.eu/about

And part of the research project NICESHIP sponsored by the Spanish Ministry of Science and Innovation under Grant RTI2018-094744-B-C21.

REFERENCES

Hull structural design - Ships with length 100 metres and above. Technical report, DNV, 2016. URL `www.dnvgl.com`.

Car, E., Oller, S., and Oñate, E. (2000). An anisotropic elastoplastic constitutive model for large strain analysis of fiber reinforced composite materials. *Computer Methods in Applied Mechanics and Engineering*, 185(2-4):245–277. ISSN 00457825. doi: 10.1016/S0045-7825(99)00262-5.

Chaves, E. W. V. *Notes on Continuum Mechanics*. Lecture Notes on Numerical Methods in Engineering and Sciences. Springer Netherlands, Dordrecht, 2013. ISBN 978-94-007-5985-5. doi: 10.1007/978-94-007-5986-2. URL `http://link.springer.com/10.1007/978-94-007-5986-2`.

Chippendale, R. D., Golosnoy, I. O., and Lewin, P. L. (2014). Numerical modelling of thermal decomposition processes and associated damage in carbon fibre composites. *Journal of Physics D: Applied Physics*, 47(38):385301. ISSN 13616463. doi: 10.1088/0022-3727/47/38/385301. URL http://stacks.iop.org/0022-3727/47/i=38/a=385301http://stacks.iop.org/0022-3727/47/i=38/a=385301?key=crossref.e8e3fa511892bfff723543822db41f64.

Coussy, O. *Poromechanics*. John Wiley & Sons, Ltd, Chichester, UK, 12 2003. ISBN 9780470092712. doi: 10.1002/0470092718. URL http://doi.wiley.com/10.1002/0470092718.

Dodds, N., Gibson, A. G., Dewhurst, D., and Davies, J. M. (2000). Fire behaviour of composite laminates. *Composites Part A: Applied Science and Manufacturing*, 31(7):689–702. ISSN 1359835X. doi: 10.1016/S1359-835X(00)00015-4.

Feih, S., Mathys, Z., Gibson, A. G., and Mouritz, A. P. (2006). Modelling the tension and compression strengths of polymer laminates in fire. doi: 10.1016/j.compscitech.2006.07.038. URL www.elsevier.com/locate/compscitech.

Feih, S., Mathys, Z., Gibson, A. G., and Mouritz, A. P. (2007). Modelling the compression strength of polymer laminates in fire. *Composites Part A: Applied Science and Manufacturing*, 38(11):2354–2365. doi: 10.1016/j.compositesa.2007.04.013.

Gibson, A. G., Wu, Y. S., Chandler, H. W., Wilcox, J. A. D., and Bettess, P. (1995). A Model for the Thermal Performance of Thick Composite Laminates in Hydrocarbon Fires. *Revue de l'Institut Français du Pétrole*, 50(1):69–74. ISSN 0020-2274. doi: 10.2516/ogst:1995007. URL http://ogst.ifpenergiesnouvelles.fr/10.2516/ogst:1995007.

Gibson, A. G., Wright, P. N. H., Wu, Y. S., Mouritz, A. P., Mathys, Z., and Gardiner, C. P. (2004). The Integrity of Polymer Composites during and after Fire. *Journal of Composite Materials*, 38(15):1283–1307. ISSN 0021-9983. doi: 10.1177/0021998304042733. URL http://journals.sagepub.com/doi/10.1177/0021998304042733.

Green, A. E. and Naghdi, P. M. (1965). A Dynamical theory of interacting continua. *International Journal of Engineering Science*, 3(2):231–241. ISSN 00207225. doi: 10.1016/0020-7225(65)90046-7.

Henderson, J. B. and Hagen, S. C. (1985). A radiant heat flux apparatus for measuring the thermal response of polymeric materials to high temperatures. *Polymer Composites*, 6(2):110–114. ISSN 0272-8397. doi: 10.1002/pc.750060209. URL http://doi.wiley.com/10.1002/pc.750060209.

Henderson, J. and Wiecek, T. (1987). A Mathematical Model to Predict the Thermal Response of Decomposing, Expanding Polymer Composites. *Journal of Composite Materials*, 21(4):373–393. ISSN 0021-9983. doi: 10.1177/002199838702100406. URL http://journals.sagepub.com/doi/10.1177/002199838702100406.

Henderson, J., Wiebelt, J., and Tant, M. (1985). A Model for the Thermal Response of Polymer Composite Materials with Experimental Verification. *Journal of Composite Materials*, 19(6):579–595. ISSN 0021-9983. doi: 10.1177/002199838501900608. URL http://journals.sagepub.com/doi/10.1177/002199838501900608.

Liu, G. R. and Quek, S. S. *The Finite Element Method: A Practical Course: Second Edition*. Elsevier Ltd., 2013. ISBN 9780080983561. doi: 10.1016/C2012-0-00779-X.

Looyeh, M. R. and Bettess, P. (1998). A finite element model for the fire-performance of GRP panels including variable thermal properties. *Finite Elements in Analysis and Design*, 30(4):313–324. ISSN 0168874X. doi: 10.1016/S0168-874X(98)00036-5.

Lua, J., O'Brien, J., Key, C. T., Wu, Y., and Lattimer, B. Y. (2006). A temperature and mass dependent thermal model for fire response prediction of marine composites. *Composites Part A:*

Applied Science and Manufacturing, 37(7):1024–1039. ISSN 1359835X. doi: 10.1016/j.compositesa.2005.01.034.

Mcgrattan, K., Hostikka, S., Mcdermott, R., Floyd, J., Weinschenk, C., and Overholt, K. NIST Special Publication 1018 Sixth Edition Fire Dynamics Simulator Technical Reference Guide Volume 1: Mathematical Model. Technical report.

Mindlin, R. D. Influence of Rotatory Inertia and Shear on Flexural Motions of Isotropic, Elastic Plates. In *The Collected Papers of Raymond D. Mindlin Volume I*, pages 225–232. Springer New York, 1989. doi: 10.1007/978-1-4613-8865-4{_}29.

Mouritz, A. P. and Gibson, A. G. *Fire Properties of Polymer Composite Materials*, volume 143 of *Solid Mechanics and Its Applications*. Springer Netherlands, Dordrecht, 2006. ISBN 978-1-4020-5355-9. doi: 10.1007/978-1-4020-5356-6. URL `http://link.springer.com/10.1007/978-1-4020-5356-6`.

Mouritz, A. P. and Mathys, Z. Post-fire mechanical properties of marine polymer composites. In *Composite Structures*, volume 47, pages 643–653. Elsevier Science Ltd, 12 1999. doi: 10.1016/S0263-8223(00)00043-X.

Mouritz, A. P. and Mathys, Z. (2000). Mechanical properties of fire-damaged glass-reinforced phenolic composites. *Fire and Materials*, 24(2):67–75. ISSN 1099-1018. doi: 10.1002/1099-1018(200003/04)24:2<67::AID-FAM720>3.0.CO;2-0.

Mouritz, A. P. and Mathys, Z. (2001). Post-fire mechanical properties of glass-reinforced polyester composites. *Composites Science and Technology*, 61(4):475–490. ISSN 02663538. doi: 10.1016/S0266-3538(00)00204-9.

Mouritz, A. P., Feih, S., Kandare, E., Mathys, Z., Gibson, A. G., Des Jardin, P. E., Case, S. W., and Lattimer, B. Y. (2009). Review of fire structural modelling of polymer composites. *Composites Part A: Applied Science and Manufacturing*, 40(12):1800–1814. ISSN 1359835X. doi: 10.1016/j.compositesa.2009.09.001. URL `http://dx.doi.org/10.1016/j.compositesa.2009.09.001`.

Oñate, E. (1994). A review of some finite element families for thick and thin plate and shell analysis.

Oñate, E. Structural Analysis with the Finite Element Method Linear Statics Volume 2. Beams, Plates and Shells. In *Springer*, volume First Edit, chapter 11, pages 675–728. 2013. ISBN 9781402087325. doi: 10.1007/978-1-4020-8743-1. URL `http://medcontent.metapress.com/index/A65RM03P4874243N.pdf`.

Rastellini, F., Oller, S., Salomón, O., and Oñate, E. (2008). Composite materials non-linear modelling for long fibre-reinforced laminates. *Computers & Structures*, 86(9):879–896. ISSN 00457949. doi: 10.1016/j.compstruc.2007.04.009. URL `https://linkinghub.elsevier.com/retrieve/pii/S0045794907001642`.

Reissner, E. (1945). The effect of transverse shear deformation on the bending of elastic plates. *J. Appl. Mech.*, pages A69–A77.

Reuss, A. (1929). Berechnung der Fließgrenze von Mischkristallen auf Grund der Plastizitätsbedingung für Einkristalle . *ZAMM - Journal of Applied Mathematics and Mechanics / Zeitschrift für Angewandte Mathematik und Mechanik*, 9(1):49–58. ISSN 15214001. doi: 10.1002/zamm.19290090104. URL `http://doi.wiley.com/10.1002/zamm.19290090104`.

Voigt, W. (1889). Ueber die Beziehung zwischen den beiden Elasticitätsconstanten isotroper Körper. *Annalen der Physik*, 274(12):573–587. ISSN 15213889. doi: 10.1002/andp.18892741206. URL `http://onlinelibrary.wiley.com/doi/10.1002/andp.18892741206/abstract`.

Wickstrom Ulf, S. N., Duthinh, D., and Mcgrattan, K. (2007). Adiabatic Surface Temperature for Calculating Heat Transfer To Fire Introduction. *Most*, 2. URL https://www.nist.gov/publications/adiabatic-surface-temperature-calculating-heat-transfer-fire-exposed-structures.